First Principles Study of Hydrated/Hydroxylated TiO_2 Nanolayers: From Isolated Sheets to Stacks and Tubes

Maurizio Casarin,[†] Andrea Vittadini,[†,*] and Annabella Selloni[‡]

[†]Istituto di Scienze e Tecnologie Molecolari del CNR (ISTM-CNR) and CR—INSTM "Village", Dipartimento di Scienze Chimiche, Università di Padova, *via* Marzolo 1, I-35131 Padova, Italy, and [‡]Chemistry Department, Princeton University, Princeton, New Jersey 08540

ABSTRACT Periodic density functional calculations are carried out to investigate the structure and the stability of hydrated/hydroxylated TiO_2 layered compounds, nanosheets, and nanotubes. Due to a very efficient interlayer hydrogen bonding, the ABA-stacked "step 3" $H_2Ti_3O_7$ compound is found to be the most stable bulk phase, in agreement with the experiment. For *single* sheets in a water-rich environment other forms are instead favored, all close in energy, namely, "step 2" titanates, hydroxylized-anatase-like layers, and lepidocrocite-TiO_2. Finally, it is shown that a lepidocrocite-TiO_2 sheet, when hydroxylated only on one side, spontaneously forms a scroll-like nanotube. The nanotube diameter estimated from our models perfectly matches the ~3 nm value observed for the internal diameters of Na-free titania nanotubes.

KEYWORDS: titanium dioxide · titanates · nanosheets · nanotubes · density functional calculations

TiO_2-based nanomaterials have been intensely investigated over the past decade.[1,2] In particular, titania nanotubes (TNTs) are attracting considerable attention as their unique properties make them potentially interesting for various applications, such as catalysis, photocatalysis, electrocatalysis, gas storage, gas sensing, and photovoltaics.[1,2]

TiO_2 nanotubes can be obtained either in Na-containing or in Na-free form; these two forms differ substantially in photoactivity.[3] Whereas for Na-containing nanotubes a description based on the stepped titanate structure is widely accepted, for the Na-free form, which is the one considered in this work, a general consensus has not yet been reached. A particularly debated issue concerns the role of hydrogen: whereas NMR indicates its absence,[4] photoelectronic properties suggest that OH groups are present.[3] In fact, models so far proposed include pure TiO_2 (in the anatase[5−8] TiO_2—B,[9] or lepidocrocite form[10]), protonated titanates such as $H_2Ti_3O_7$,[11,12] and hydroxylated (001)-oriented anatase bilayers.[4] The emerging picture is rather confusing, as all the above cited models have been claimed to fit at least one experiment.

Theoretical work on TNTs has been so far limited. On the basis of density functional theory (DFT) calculations in the local density approximation (LDA), Zhang *et al.*[13] proposed that an $H_2Ti_3O_7$ sheet bends because of the tensions arising from a partial deprotonation of one of its surfaces. However, this model has been criticized on the basis of recent experiments findings.[14,15] Moreover, extension of this model to *Na-free* TNTs runs into several difficulties. First of all, the predicted nanotube diameter (~8 nm) is significantly larger than the *internal* diameters measured for Na-free TNTs (3−5 nm)[16] Second, interwall Coulomb repulsions are likely to destabilize multiwall TNTs. To solve this issue, Zhang *et al.* suggested a coupling between the nanotube walls and assumed a partial charge compensation by surrounding Na^+ ions. However the latter argument does not hold for Na-free TNTs. Furthermore, recent measurements of the nanotube interlayer distance by Pradhan *et al.*[16,17] indicate that the value given by XRD (1.0 nm) is considerably larger than that (0.78 nm) obtained under the high vacuum conditions of TEM experiments.[18] These findings seem to rule out a strong role for interwall coupling in the stabilization of Na-free TNTs. Models based on *pure* TiO_2 were investigated by Enyashin and Seifert[19] using tight-binding DFT calculations. They found that lepidocrocite-structured nanotubes, particularly those of the (*n*,0) type, are characterized by a larger strain energy than those formed by rolling thinner anatase (101) sheets. So far,

*Address correspondence to andrea.vittadini@unipd.it.

Received for review September 23, 2008 and accepted January 20, 2009.

Published online January 29, 2009.
10.1021/nn800608n CCC: $40.75

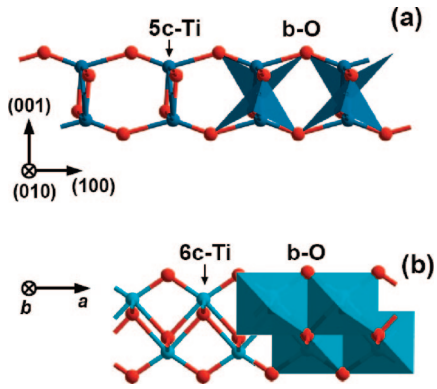

Figure 1. Mixed ball-and-stick and polyhedral representations of the structure of (a) an anatase-TiO_2(001) oriented bilayer with lattice constants fixed to those of the bulk; (b) a lepidocrocite-TiO_2 sheet.

however, this model has not been supported by experimental evidence.

Anatase-TiO_2, lepidocrocite-TiO_2 (Figure 1), and protonated titanates like $H_2Ti_3O_7$ (Figure 2), all proposed as possible constituents of nanotubes, have a close structural relationship. For instance, first principles studies have found that bilayer (001)-oriented anatase films *spontaneously* rearrange to the lepidocrocite form through a barrierless pathway.[20,21] There are two main reasons for this rearrangement: (a) the 5-fold undercoordinated (5c-Ti) cations are converted to *fully* (6-fold) coordinated 6c-Ti cations and (b) the large bond angle at the bridging oxygens (b-O), which induces a tensile stress at the anatase (001) surface,[22] is considerably reduced. These findings have been confirmed by molecular dynamics calculations by Alvarez-Ramirez and Ruiz-Morales,[23] who also found that a conversion into a stepped structure can easily occur as well. This is a system which can be viewed as made of lepidocrocite-like ribbons of edge-sharing octahedra interrupted by steps,[24] that are caused by the insertion of OH groups.

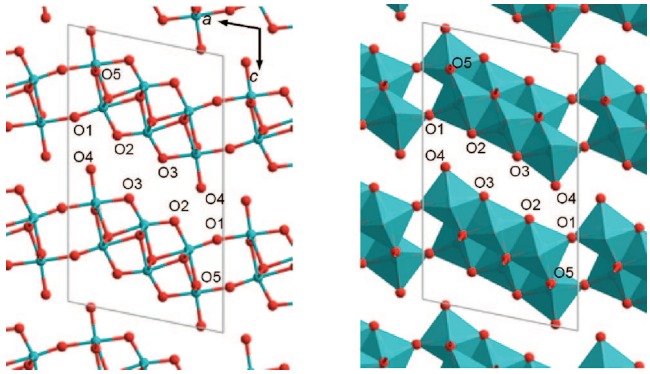

Figure 2. The framework structure of $H_2Ti_3O_7$ shown in a ball-and-stick (left) and in a polyhedral representation (right) after ref 24. The gray line marks the border of the nonprimitive monoclinic cell. The numbering scheme used to indicate sites for proton absorption is also displayed. O1 is denoted as the "step" b-O site/ion, whereas O2 and O3 are denoted as the "ribbon" b-O ions/sites. Note that, in order to allow an easier comparison of the structural parameters with those of the nanosheets, a nonstandard setting has been chosen for the axes (*a* and *c* have been interchanged).

For instance, $H_2Ti_3O_7$ (see Figure 2) is defined as a "step 3" titanate since steps are separated by *three* edge-sharing octahedra.[23,25] For each kind of stepped structure, however, several atomic configurations are possible, depending on the arrangement of the protons at the different O sites. The specific proton pattern not only determines the intrinsic stability of the nanosheet, but also affects the interlayer interactions which are dominated by hydrogen bonds (absent in the case of lepidocrocite-TiO_2). Since interlayer H-bonds are likely to be present also in TNTs, it is important to investigate how the proton pattern influences the stability as well the other physicochemical properties of TiO_2 nanosheets.

In this work, we present first principles calculations on isolated sheets and stacked crystals with different stoichiometries, with special focus on the effects of various proton patterns on the system structure and stability. On the basis of these calculations, we propose a new model for Na-free TNTs, based on an anatase/lepidocrocite sheet, where water dissociation is allowed to occur only on one side.

RESULTS AND DISCUSSION

Single and Stacked Sheets of $H_2Ti_3O_7$ Stoichiometry. Previous DFT calculations on the stability of $H_2Ti_3O_7$ nanosheets[13] were carried out at the LDA level, which is known to overestimate the strength of hydrogen bonds by ~70%.[26] Moreover, only AAA-stacked $H_2Ti_3O_7$ sheets (Figure 3) were considered and the contributions of intralayer effects and interlayer hydrogen bonds were not distinguished.

Seven nonequivalent oxygen sites are present in the framework structure of step-3 titanates (Figure 2): one 1-fold coordinated, three "bridging" 2-fold coordinated (b-O), one 3-fold coordinated (t-O), and two 4-fold sites. Using the labeling scheme of Feist and Davies,[24] we denote the 1-fold coordinated oxygen O4 (see Figure 2). To limit the number of configurations to be investigated, we assumed that, because of its basicity, the O4 anion always carries at least one proton, that is, an O4−H moiety is always present. This can be considered as the hydroxide anion resulting from an hypothetical H_2O dissociation on the TiO_2 nanosheet:

$$3TiO_2 + H_2O \rightarrow H_2Ti_3O_7 \qquad (1)$$

With the above assumption, the various proton configurations of the sheet can be labeled by specifying only the site for the proton released in the H_2O dissociation, *viz*. H@O*i*/O*j* denotes a configuration with a proton at O*i* on one side of the sheet, and a proton at O*j* on the other side (a proton at O4 is also present on each side). At variance with previously reported calculations, in this work we consider also *mixed* configurations, where protons are arranged in different fashions at the two sides of the sheet.

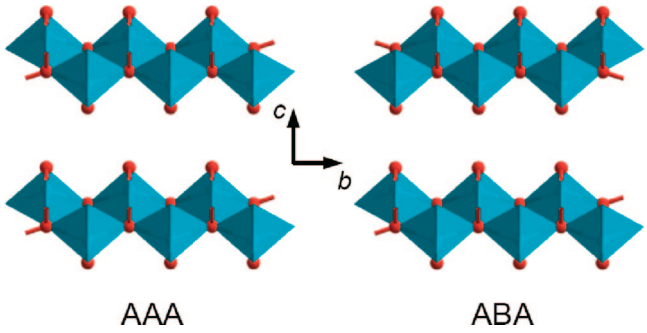

Figure 3. Polyhedral representations of a layered titanate in a AAA (left) and in a ABA (right) stacking.

All energies are referred to a formula unit and, for a slab model of $(H_2Ti_xO_{2x+2})_y$ composition, are calculated as

$$E = [E(\text{slab}) - x \cdot E(TiO_2) - E(H_2O)] / y \qquad (2)$$

where E(slab) is the total energy of the slab model, $E(TiO_2)$ is the total energy of a TiO_2 unit in an isolated lepidocrocite-structured nanosheet, and $E(H_2O)$ is the total energy of an isolated H_2O molecule.

In the case of *isolated* $H_2Ti_3O_7$ sheets (see Figure 4), we find that b-O sites are largely favored over higher-coordinated O sites, in agreement with ref 13. In fact, our calculations show that the H@O5/O5 configuration is unstable ($E = +0.18$ eV). Moreover, several stable proton configurations turn out to be distributed over a narrow (~0.2 eV) energy interval, with *ribbon* b-O sites generally favored over O1, the *step* b-O site. In the latter case, the H@O1/O1 trititanate-type configuration is only a local minimum: the most stable configuration, H@O1/O1*, is actually disrupted into hydrogen-bonded anatase/lepidocrocite-like nanoribbons. Also remarkable is the spontanoues rearrangement of the H@O4/O4 configuration into a flat, lepidocrocite-structured nanosheet, on which weakly adsorbed molecular water is present. The stability of this system suggests that single sheets of protonated titanates could possibly rearrange into lepidocrocite-TiO_2, confirming the results of previous simulations.[23] This aspect will be discussed in more detail in the next section.

Stabilities and structural parameters for the AAA-stacked systems are summarized in Table 1. A comparison with the isolated sheet energies, also reported in Figure 4, allows us to estimate that the AAA stacking interaction amounts to 0.3 eV. This means that the average strength of the interlayer H-bonds amounts to ~0.15 eV. At variance with the monolayer case, the H@O4/O4 configuration maintains a stepped structure, that is, no transition to the lepidocrocite structure is predicted to occur. The energy ordering, E(O3/O3) < E(O4/O4) < E(O2/O2) < E(O1/O1), is different from the LDA result[13] E(O2/O2) < E(O1/O1) ≪ E(O3/O3). Also, the values for the *c* parameter are ~11% smaller than those reported in ref 13.[27] These discrepancies between our PBE and the LDA calculations can be attributed to the fact that the LDA calculations were carried out with the symmetry constraints of the *P*21/*M*(11) space group, which force the hydroxyls to be parallel to the {010} crystallographic planes. This prevents the formation of interlayer hydrogen bonds, since in the AAA stacking the closest oxygens belonging to facing surfaces are shifted by *b*/2. In fact, our calculations of fully relaxed AAA-stacked systems confirm that a more favorable arrangement can be achieved by allowing the directions of the O−H bonds to deviate from {010} planes (see, *e.g.*, the structure of the H@O3/O3 configuration in Figure 5).

For the ABA-stacked structures, very large rearrangements take place upon structural optimization. For instance, the symmetric ABA-H@O2/O2 proton configuration spontaneously evolves to the ABA-H@O2/O4 asymmetric one, while the ABA-H@O3/O3 configuration is unstable with respect to the AAA-stacked structure. Among the identified ABA local minima structures (Table 2), only one, H@O1/O1, corresponds to a symmetric structure. These ABA local minima are spread over a larger energy interval with respect to the AAA ones (0.5 *vs* 0.3 eV), and the ABA absolute minimum is 0.3 eV lower than that found for the AAA case. The most stable ABA-stacked H@O3/O4 and H@O2/O3 configurations have quite similar lattice constants, which are in both cases very close (deviations <1%) to the experimental values.[24] Inspection of the atomic structures (Figure 6) reveals that the protons are ideally lined up to allow the formation of strong O2···O4, O3···O3, and O4···O4 hydrogen bonds. This H-bonding scheme, suggested also by powder neutron diffraction

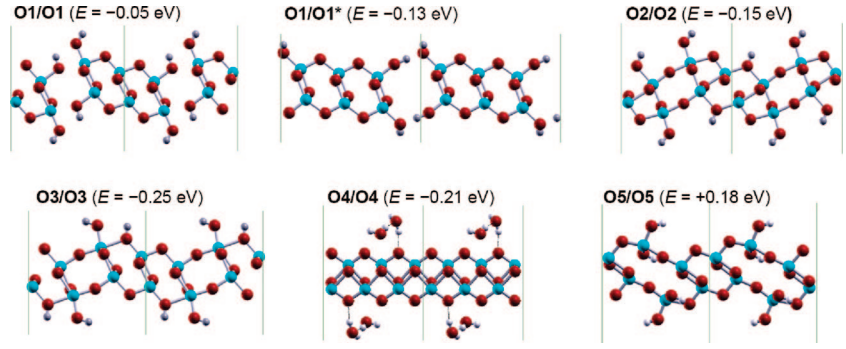

Figure 4. Computed equilibrium structures and energies of an isolated $H_2Ti_3O_7$ sheet. The corresponding lattice parameters (in Å) are: O1/O1 (a = 9.639, b = 3.725); O1/O1* (a = 11.376, b = 3.962); O2/O2 (a = 9.352, b = 3.711); O3/O3 (a = 9.552, b = 3.746); O4/O4 (a = 9.060, b = 7.460); O5/O5: (a = 9.188, b = 3.816). The following (not shown) mixed configurations were also computed: O1/O3 (E = −0.15, a = 9.592, b = 3.780); O2/O3 (E = −0.20, a = 9.412, b = 3.763); O3/O4 (E = −0.13, a = 9.514, b = 3.755).

TABLE 1. Stabilities (per formula unit, see eq 2) and Optimized Parameters for Models of $H_2Ti_3O_7$ in the AAA Stacking with Different Proton Configurations (note that a nonstandard axis setting has been chosen)

	E (eV)	*a* (Å)	*b* (Å)	*c* (Å)	β (deg)
01/01	−0.23	9.638	3.723	7.840	102.97
02/02	−0.41	9.229	3.764	7.910	101.69
03/03	−0.53	9.406	3.763	7.973	106.93
04/04	−0.49	9.342	3.796	7.800	105.01
01/01[a]	(−7935.2)	9.759	3.734	8.771	104.42
02/02[a]	(−7935.3)	9.545	3.764	8.998	102.65
03/03[a]	(−7934.0)	-	-	-	-

[a]LDA values from ref 13. Values in parentheses are total energies, which depend on the specific computational setup (pseudopotentials, *etc.*) and so cannot be directly compared to our results.

data,[24] is able to zip together titanate sheets very efficiently, explaining why protonated titanates, unlike alkaline titanates, prefer the ABA stacking sequence. The role of H-bonding in stabilizing the H@O3/O4 and H@O2/O3 structures can be also inferred from the fact that these configurations do not exhibit an enhanced stability if taken as single sheets ($E = -0.13$, and $E = -0.20$ eV, respectively).

The stability of the ABA-stacked H@O3/O4 configuration suggests that undissociated water molecules can occur in protonated titanates (see Figure 6), even in the absence of intercalated water. As these undissociated water molecules are likely to desorb more readily with respect to dissociated ones, they could play a role in the $H_2Ti_3O_7 \rightarrow TiO_2$ (B) transition, which is found to start with the reaction $2H_2Ti_3O_7 \rightarrow H_2Ti_6O_{13} + H_2O(g)$.[24]

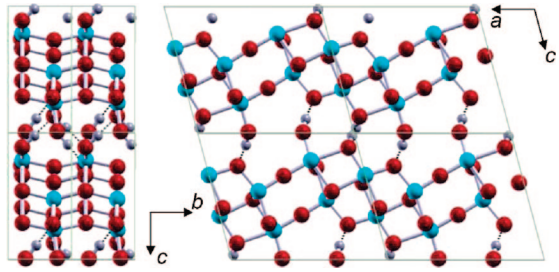

Figure 5. Equilibrium structure for the O3/O3 proton configuration of $H_2Ti_3O_7$ in the AAA stacking sequence.

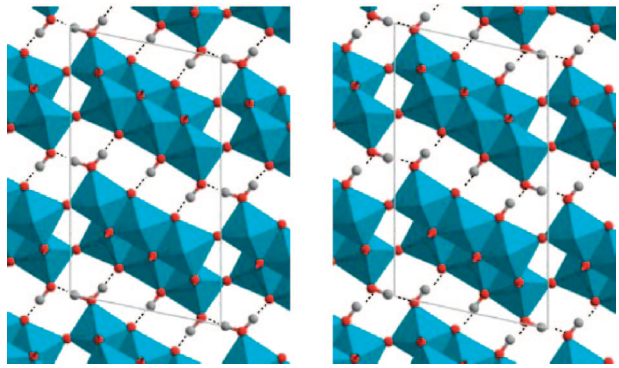

Figure 6. Polyhedral representations of the O3/O4 (left) and of the O2/O3 (right) proton configurations of ABA-stacked $H_2Ti_3O_7$.

TABLE 2. Stabilities (per formula unit, see eq 2) and Optimized Lattice Parameters for Models of $H_2Ti_3O_7$ in the ABA Stacking with Different Proton Configurations

	E (eV)	*a* (Å)	*b* (Å)	*c* (Å)	β (deg)
01/01	−0.38	9.639	3.716	15.841	96.54
01/03	−0.48	9.350	3.762	16.168	100.16
02/04	−0.55	9.355	3.770	16.181	100.48
02/03	−0.82	9.271	3.768	16.189	102.16
03/04	−0.85	9.252	3.773	16.147	101.67
exptl.[a]		9.188	3.747	16.025	101.46

[a]From ref 24.

In the strongly bonded multilayer structures of Figure 6, all the protons are involved in interlayer H- bonds. Moreover, each one-fold coordinated O4 atom participates in two hydrogen bonds, either as a double donor or as a donor−acceptor, whereas all ribbon b-O atoms are involved in one H-bond only, either as donors or as acceptors. This is a special property of the $H_2Ti_3O_7$ titanate. In fact, for $H_2Ti_nO_{2n+1}$ with $n > 3$, some of the b-O ions cannot participate in H-bonds because the number of protons available on the opposite surface is insufficient. Similarly, a less efficient interlayer hydrogen bonding can be expected also for a "step 2" $H_2Ti_2O_5$ titanate, because of the low density of *ribbon* b-O acceptors.

Single and Stacked Sheets of $H_2Ti_2O_5$ Stoichiometry. Although (to our best knowledge) step-2 protonated titanates do not actually exist, they are interesting to consider because the $H_2Ti_2O_5$ stoichiometry is the one expected for a fully hydroxylated (001)-oriented anatase nanolayer (water is known to dissociatively adsorb on anatase (001) up to a saturation coverage of 0.5 ML,[28] implying that water-saturated (001)-oriented anatase nanolayers has a $H_2Ti_2O_5$ stoichiometry), which has been recently proposed as a structural model for TiO_2 nanosheets on the basis of X-ray diffraction (XRD) data.[4] A sketch of the structure of an hypothetical step-2 H_2TiO_5 solid is shown in Figure 7, where the used numbering of the O atoms is also shown.

Our results for $H_2Ti_2O_5$ nanosheets are summarized in Figure 8. The most stable configurations are a stepped O2/O2 structure (−0.32 eV), an hydroxylated-anatase-like O1/O1** structure (−0.28 eV) and a "wet-lepidocrocite" O3/O3 configuration (−0.25 eV), all close in energy. By comparing the results in Figures 4 and 8 we can see that, for single sheets, the $H_2Ti_2O_5$ stoichiometry is favored over the $H_2Ti_3O_7$ one. Furthermore, our results are compatible with X-ray determinations indicating that the lepidocrocite structure is actually preferred for isolated nanosheets.[29] In fact, the "wet-lepidocrocite" O3/O3 structure is quite close to the absolute minimum and its small energy cost could be easily overcome by entropic effects. Given the facile interconversion between lepidocrocite and anatase,[20] the O1/O1** and O3/O3 sheets are closely related to the structures of *dissociatively* and *molecularly* adsorbed

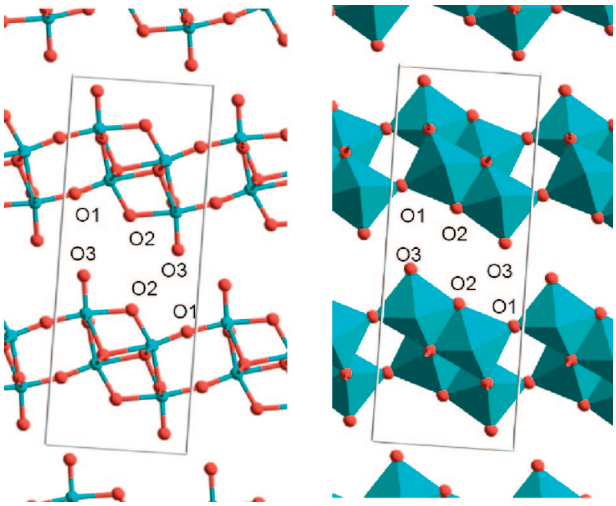

Figure 7. The framework structure of an hypothetical step-2 $H_2Ti_2O_5$ compound, shown in a ball-and-stick (left) and in a polyhedral representation (right).

water on the anatase (001) surface. Interestingly, the strong preference for dissociative water adsorption found for the anatase (001) surface[28] becomes almost negligible in the nanosheet case.

Additional calculations for both AAA- and ABA-stacked step-2 titanate structures are reported in Table 3. As observed for the step-3 case, some configurations become drastically modified during the optimization. No clear preference is present for the ABA stacking in this case. Overall, these calculations show that whereas for *stacked* titanates an efficient H-bonding makes the $H_2Ti_3O_7$ stoichiometry favored over the $H_2Ti_2O_5$ one, no such preference can be found as far as *single* protonated sheets are considered.

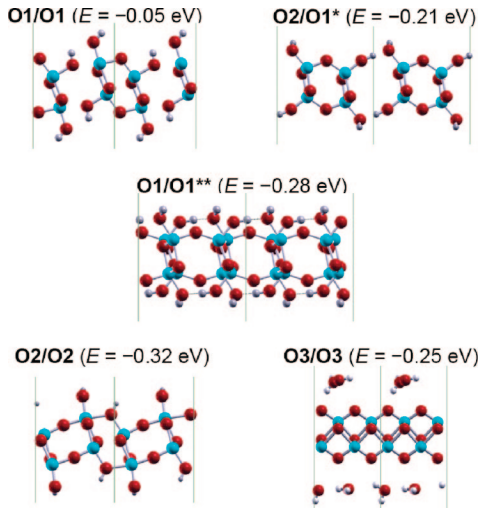

Figure 8. Equilibrium structures for a single $H_2Ti_2O_5$ sheet. The corresponding lattice parameters (in Å) are: O1/O1 (a = 6.780, b = 3.700); O1/O1* (a = 8.217; b = 3.71); O1/O1 (a = 8.130; b = 7.210); O2/O2 (a = 6.544; b = 3.755); O3/O3 (a = 6.060; b = 7.460). Configurations O1/O1** and O3/O3 are described by 1 × 2 supercells. A mixed O1/O2 configuration (not shown) was also computed (E= −0.17, a = 6.681, b = 3.735).**

Nanotube Models. Independent of its formation *mechanism* (which we do not intend to investigate here), a *stable* nanotube is formed only if the framework structure of the sheet is able to sustain the strain arising from the different surface tensions existing at the two sides of the sheet. In principle, a nanotube with low strain energy can be obtained from a nanosheet whose surfaces have different optimal values of the lattice parameter along the scrolling direction, as in the partially deprotonated trititanate model of ref 11. On the basis of the results presented so far, it appears that this requirement could be satisfied by a *neutral* sheet made by coupling the hydroxylized-anatase-like H_2TiO_5(O1/O1)** and wet-lepidocrocite H_2TiO_5(O3/O3) configurations (which are closely related, but have largely different a structural parameters).

To confirm the above conjecture, we performed calculations on three nanoribbon models, which, with reference to the lepidocrocite structure shown in Figure 1, included 2 cells along b, and a total of 3, 5, and 7 cells along a. In practice, these models were built starting from the $H_2Ti_2O_5$(O1/O1)** configuration, by removing water molecules from the top surface, which means that they have a $H_2Ti_4O_9$ stoichiometry. To minimize size effects, the dangling bonds of the lateral surfaces of the nanoribbons were terminated with OH groups[30−32] obtained from the dissociative adsorption of water molecules. Only the Γ point was used, and the b constant (the periodicity along a is lost in the nanoribbon models) was optimized on a coarse 0.05 Å grid (because of the approximated nature of the models, it makes little sense to perform calculations of higher accuracy). As a check, analogous calculations were run on nanoribbon models representing lepidocrocite-TiO_2 sheets, and fully hydroxylized anatase bilayers, *viz.* the H_2TiO_5(O1/O1)** sheet. The optimized structures for the largest models of all investigated systems are shown in Figure 8. To estimate the convergence of the results, we computed the energy corresponding to the lepidocrocite-TiO_2 + H_2O → H_2TiO_5(O1/O1)** transformation. This changed from 0.33 to 0.29 and 0.29 eV/H_2O for nanoribbons of 2 × 3

TABLE 3. Stabilities (per formula unit, see eq 2) and Optimized Lattice Parameters for Models of a Hypothetical Step-2 Layered Compound of $H_2Ti_2O_5$ Stoichiometry

	E (eV)	a (Å)	b (Å)	c (Å)	β (deg)
ABA stacking					
01/01	−0.35	6.750	3.671	15.697	93.72
02/02	−0.64	6.496	3.773	16.221	93.80
01/02	−0.52	6.601	3.741	16.026	93.12
AAA stacking					
02/02	−0.69	6.553	3.779	7.742	100.54
03/03	−0.64	6.506	3.833	7.690	100.18

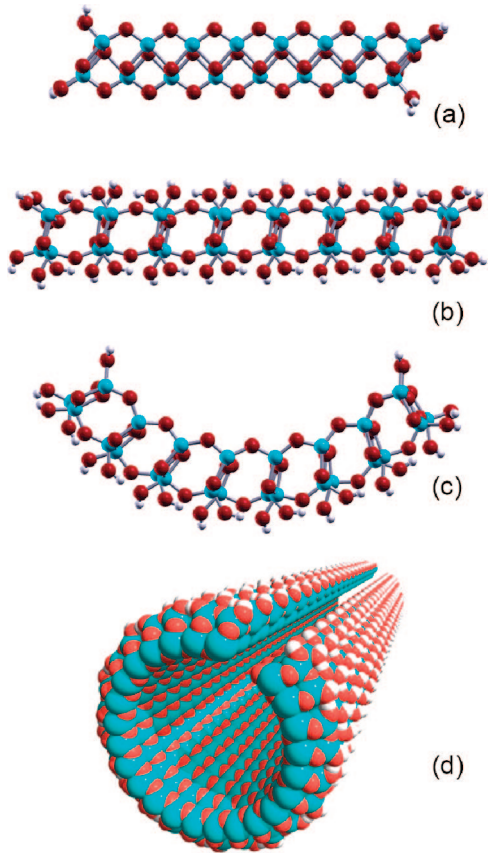

Figure 9. Side views of the equilibrium structures of the largest nanoribbon models representing (a) a clean lepidocrocite sheet; (b) a fully hydroxylated sheet; (c) a sheet hydroxylated only on the bottom surface (used to model a portion of scrolled nanotube); (d) a space-filling representation of a scrolled nanotube built from the atomic coordinates of the central part of the nanoribbon model shown in panel c.

to 2 × 5, and 2 × 7 size, respectively. This indicates that medium-size models are already a realistic representation of the extended sheets, for which a transformation energy of 0.28 eV/H_2O value is obtained (see Figure 7).

In tune with our expectations, our results show that whereas the equilibrium structures of the lepidocrocite-like and of the fully hydroxylated models are perfectly planar (see Figures 9a and 9b), the asymmetrically hydroxylated models are significantly bent (see Figure 9c). Morevorer, the framework structure of the latter could be described as an anatase-like bilayer distorted toward lepidocrocite. This could explain why both anatase- and lepidocrocite-like models are able to fit experiments. The diameter *D* of the complete nanotube was estimated by fitting the positions of the most internal 3-fold coordinated O ions with the equation of a circle. We obtained $D = 33 \pm 6$ Å, 27 ± 1 Å, and 27.0 ± 0.4 Å for increasing nanoribbon size, which confirms that the medium-size ribbons are reasonable models of the extended system. A complete single-wall nanotube was built by propagating the coordinates of the central part of the nanoribbon model, see Figure 9d. Our predictions agree very well with the ~3 nm *internal* diameter measured for typical TiO_2 nanotubes (see, *e.g.*, ref 16 and 17). *External* nanotube diameters can be up to 1 order of magnitude larger,[33] which implies a substantial increase of the curvature radius on moving from the inner to the outer part of the nanotube. This effect can be easily introduced in our model, by allowing a smaller concentration of dissociated water in the outer nanotube layers, which is compatible with the indications of NMR experiments.[4]

Finally, It is also interesting to consider the strain energy of the nanotube. This can be indirectly estimated by computing the energy corresponding to the transformation: lepidocrocite-ribbon + $nH_2O \rightarrow$ curved-ribbon (*e.g.*, the process where the structure of Figure 9a is converted into the structure of Figure 9b). The resulting energy is *negative* (*i.e.*, the process is exothermic), and amounts to 0.35, 0.28, and 0.25 eV/H_2O. This means that the stability of the scroll-like nanotube is not far from that of the planar sheets even when neglecting interwall interactions, that is the strain energy of the nanotube is very low.

SUMMARY AND CONCLUSIONS

In conclusion, we have investigated the structure and stability of single/stacked TiO_2-based nanosheets of various stoichiometries. Among stacked systems, ABA-type $H_2Ti_3O_7$ is computed to be most stable, with lattice parameters in very good agreement with the experiment. The ABA stacking is favored because it allows a very efficient interlayer hydrogen bonding. As far as single sheets are concerned, the $H_2Ti_3O_7$ stoichiometry is no more favored. Instead, the following systems are found to be most stable and close in energy: (i) step-2 titanate layers; (ii) hydroxylated anatase (001)-like sheets; (iii) lepidocrocite-TiO_2 sheets weakly interacting with water. Finally, on the basis of the strong dependence of the *a* parameter of single sheets on the water adsorption mode, we suggest a new model for Na-free scroll-like TiO_2 nanotubes, where the strain energy is minimized by an unbalanced degree of water dissociation at the two sides of the sheet.

METHODS

We performed periodic DFT calculations using the Perdew–Burke–Ernzerhof[34] (PBE) gradient-corrected exchange-correlation functional. A plane-wave basis set was used in conjuction with Vanderbilt ultrasoft pseudopotentials.[35] Valence states include 2s and 2p shells for O, and 3s, 3p, 3d, and 4s states for Ti.[36] Single layers of material were approximated with periodically repeated slabs, including a vacuum space of at least 12 Å. Cell parameters were optimized with a damped cell-dynamics minimization,[37] while internal ion coordinates were determined with the BFGS algorithm,[38] without symmetry constraints. In a previous study[21] we found that, in order to reproduce results of

converged fixed-cutoff calculations, variable-cell calculations require a kinetic-energy cutoff of 50 Ry for the wave functions and 400 Ry for the augmentation charge. A $2 \times 4 \times 2$ Monkhorst−Pack grid was used to sample the Brillouin zone of the primitive cell of $H_2Ti_3O_7$, and meshes of similar densities were adopted for the other systems. Test calculations showed that increasing the sampling point densities changes total energy differences by ~ 0.001 eV/TiO_2 formula unit. As a further check, we optimized the structure of $Na_2Ti_3O_7$, which has a *P21/m* symmetry. The computed parameters are in excellent agreement with the experiment[39] (values in parentheses): $a = 8.655$ (8.571) Å, $b = 3.812$ (3.804) Å, $c = 9.242$ (9.135) Å, $\alpha = 101.66°$ (101.57°). Only the Γ point was used in the calculations on the nanoribbon models.

Acknowledgment. The calculations of this work have been done with the QUANTUM-ESPRESSO package.[40] Computational resources and assistance were provided by the "Laboratorio Interdipartimentale di Chimica Computazionale" (LICC) at the Dipartimento di Scienze Chimiche of the University of Padova, and by CINECA (Bologna, Italy). Molecular graphics have been generated by XcrysDen[41] and GDIS.[42]

REFERENCES AND NOTES

1. Bavykin, D. V.; Friederich, J. M.; Walsh, F. C. Protonated Titanates and TiO_2 Nanostructured Materials: Synthesis, Properties, and Applications. *Adv. Mater.* **2006**, *18*, 2807–2824.
2. Chen, X.; Mao, S. S. Titanium Dioxide Nanomaterials: Synthesis, Properties, Modifications, and Applications. *Chem. Rev.* **2007**, *107*, 2891–2959.
3. Riss, A.; Berger, T.; Stankic, S.; Bernardi, J.; Knözinger, E.; Diwald, O. Charge Separation in Layered Titanate Nanostructures: Effect of Ion Exchange Induced Morphology Transformation. *Angew. Chem., Int. Ed.* **2008**, *47*, 1496–1499.
4. Mogilevsky, G.; Chen, Q.; Kulkarni, H.; Kleinhammes, A.; Mullins, W. M.; Wu, Y. Layered Nanostructures of Delaminated Anatase: Nanosheets and Nanotubes. *J. Phys. Chem. C* **2008**, *112*, 3239–3246.
5. Wang, F.; Jiu, J.; Pei, L.; Nakagawa, K.; Isoda, S.; Adachi, M. *Chem. Lett.* **2005**, *34*, 1238–1239.
6. Jia, Y.; Kleinhammes, A.; Kulkarni, H.; MacGuire, K.; Mc Neil, L. E.; Wu, Y. Synthesis and Characterization of TiO_2 Nanotube/Hydroquinone Hybrid Structure. *J. Nanosci. Nanotechnol.* **2007**, *7*, 458–462.
7. Morgan, D. L.; Waclawik, E. R.; Frost, R. L. Relationship of Titania Nanotube Binding Energies and Raman Spectra. In Proceedings International Conference on Nanoscience and Nanotechnology (ICONN '06), Brisbane, Q.L.D., 2006; Jagadish, C., Lu, G.Q.M., Eds.; IEEE Press: Piscataway, NJ, 2006; pp. 60−63.
8. Mogilevski, G.; Chen, Q.; Kleinhammes, A.; Wu, Y. The Structure of Multilayered Titania Nanotubes Based on Delaminated Anatase. *Chem. Phys. Lett.* **2008**, *460*, 517–520.
9. Armstrong, G.; Armstrong, A. R.; Canales, J.; Bruce, B. G. Nanotubes with the TiO_2-B structure. *Chem. Commun.* **2005**, 2454–2456.
10. Ma, R.; Bando, Y.; Sasaki, T. Nanotubes of Lepidocrocite Titanates. *Chem. Phys. Lett.* **2003**, *380*, 577–582.
11. Chen, Q.; Du, G. H.; Zhang, S.; Peng, L.-M. The Structure of Trititanate Nanotubes. *Acta Cryst. B* **2002**, *58*, 587–593.
12. Gateshki, M.; Chen, Q.; Peng, L.-M.; Chupas, P.; Petkov, V. Structure of Nanosized Materials by High-Energy X-Ray Diffraction: Study of Titanate Nanotubes. *Z. Kristallogr.* **2007**, *222*, 612–616.
13. Zhang, S.; Chen, Q.; Peng, L.-M. Structure and Formation of $H_2Ti_3O_7$ Nanotubes in an Alkali Environment. *Phys. Rev. B* **2005**, *71*, 014104-1–014104-11.
14. Bavykin, D. V.; Parmon, V. N.; Lapkin, A. A.; Walsh, F. C. The Effect of Hydrothermal Conditions on the Mesoporous Structure of TiO_2 Nanotubes. *J. Mater. Chem.* **2004**, *14*, 3370–3377.
15. Tsai, C.-C.; Teng, H. Regulation of the Physical Characteristics of Titania Nanotube Aggregates Synthesized from Hydrothermal Treatment. *Chem. Mater.* **2004**, *16*, 4352–4358.
16. Pradhan, S. K.; Mao, Y.; Wong, S. S.; Chupas, P.; Petkov, V. Atomic-Scale Structure of Nanosized Titania and Titanate: Particles, Wires, and Tubes. *Chem. Mater.* **2007**, *19*, 6180–6186.
17. Yao, B. D.; Chan, Y. F.; Zhang, X. Y.; Zhang, W. F.; Yang, Z. Y; Wang, N. Formation mechanism of TiO_2 nanotubes. *Appl. Phys. Lett.* **2003**, *82*, 281–283.
18. To explain this discrepancy, these authors proposed that the high vacuum conditions of TEM experiments cause the evaporation of the water molecules originally present in the interlayer region of the nanotube.
19. Enyashin, A. N.; Seifert, G. Structure, Stability and Electronic Properties of TiO_2 Nanostructures. *Phys. Status Solidi B* **2005**, *242*, 1361–1370.
20. Orzali, T.; Casarin, M.; Granozzi, G.; Sambi, M.; Vittadini, A. Bottom-up Assembly of Single-Domain Titania Nanosheets on (1×2)-Pt(110). *Phys. Rev. Lett.* **2006**, *97*, 156101-1–156101-4.
21. Vittadini, A.; Casarin, M. Ab Initio Modeling of TiO_2 Nanosheets. *Theor. Chem. Acc.* **2008**, *120*, 551–556.
22. Lazzeri, M.; Selloni, A. Stress-Driven Reconstruction of an Oxide Surface: The Anatase $TiO_2(001)$-(1×4) Surface. *Phys. Rev. Lett.* **2001**, *87*, 266105-1–266105-4.
23. Alvarez-Ramirez, F.; Ruiz-Morales, Y. Ab Initio Molecular Dynamics Calculations of the Phase Transformation Mechanism for the Formation of TiO_2 Titanate-Type Nanosheets from Anatase. *Chem. Mater.* **2007**, *17*, 2947–2959.
24. Feist, T. P.; Davies, P. K. The Soft Chemical Synthesis of TiO_2 (B) from Layered Titanates. *J. Solid State Chem.* **1992**, *101*, 275–295.
25. Note that in contrast to this definition, $H_2Ti_3O_7$ is defined as a "step 2" titanate in ref .
26. Hamann, D. R. H_2O Hydrogen Bonding in Density-Functional Theory. *Phys. Rev. B* **1997**, *55*, R10157–R10160.
27. Note that axes *a* and *c* have been interchanged in the present paper.
28. Vittadini, A.; Selloni, A.; Rotzinger, F. P.; Grätzel, M. Structure and Energetics of Water Adsorbed at TiO_2 Anatase (101) and (001) Surfaces. *Phys. Rev. Lett.* **1998**, *81*, 2954–2957.
29. Gateshki, M.; Hwang, S.-J.; Park, D. H.; Ren, Y.; Petkov, V. Structure of Exfoliated Nanosheets Determined by Atomic Pair Distribution Function Analysis. *Chem. Mater.* **2004**, *16*, 5153–5157.
30. Casarin, M.; Maccato, C.; Vittadini, A. Molecular Chemisorption on $TiO_2(110)$: A Local Point of View. *J. Phys. Chem. B* **1998**, *102*, 10745–10752.
31. Casarin, M.; Maccato, C.; Vittadini, A. Density functional studies of molecular chemisorption on $TiO_2(110)$. *Appl. Surf. Sci.* **1999**, *142*, 196–199.
32. Note that in contrast to surface models, where a termination is needed also at the bottom surface, plain (*i.e.*, with $Z = 1$) H atoms can be used in the present case.
33. Wei, M.; Konishi, Y.; Zhou, H.; Sugihara, H.; Arakawa, H. Formation of Nanotubes TiO_2 from Layered Titanate Particles by a Soft Chemical Process. *Solid State Commun.* **2005**, *133*, 493–497.
34. Perdew, J. P.; Burke, K.; Ernzerhof, M. Generalized Gradient Approximation Made Simple. *Phys. Rev. B* **1996**, *77*, 3865–3868.
35. Vanderbilt, D. Soft Self-Consistent Pseudopotentials in a Generalized Eigenvalue Formalism. *Phys. Rev. B* **1990**, *41*, 7892–7895.
36. Lazzeri, M.; Vittadini, A.; Selloni, A. Structure and Energetics of Stoichiometric TiO_2 Anatase Surfaces. *Phys. Rev. B* **2001**, *63*, 155409-1–155409-9.
37. Wentzcovitch, R. M. Invariant Molecular-Dynamics Approach to Structural Phase-Transitions. *Phys. Rev. B* **1991**, *44*, 2358–2361.

38. See for example: William, S. A., Press, H., Flannery, B. P., and Vetterling, W. T. *Numerical Recipes: The Art of Scientific Computing*; Cambridge University Press: Cambridge, U.K., 2007.
39. Andersson, S.; Wadsley, A. D. The Crystal Structure of $Na_2Ti_3O_7$. *Acta Crystallogr.* **1961**, *14*, 1245–1249.
40. Baroni, S.; de Gironcoli, S.; Dal Corso, A.; Giannozzi, P. Plane-Wave Self-Consistent Field, accessed June, 2008, http://www.pwscf.org/.
41. Kokalj, A. Computer Graphics and Graphical User Interfaces as Tools in Simulations of Matter at the Atomic Scale. *Comput. Mater. Sci.* **2003**, *28*, 155168;. code available from http://www.xcrysden.org/.
42. Fleming, S.; Rohl, A. GDIS: a Visualization Program for Molecular and Periodic Systems. *Z. Kristallogr.* **2005**, *220*, 580–584; code available from http://gdis.sourceforge.net/.